ADVANCED MATERIALS INTERFACES
www.advmatinterfaces.de

3D Graphene Oxide Micropatterns Achieved by Roller-Assisted Microcontact Printing Induced Interface Integral Peel and Transfer

Peng Xiao, Shiyu Du, Tao Zhang, Nianxiang Qiu, Jiawei Zhang, Youju Huang, Changjin Wan, Rainer Jordan, Qing Huang, Zhaoping Liu, and Tao Chen**

Most fascinating applications of graphene-based devices are highly dependent on the precise fabrication of patterned graphene microstructures. While considerable progress of 2D patterning of graphene has been achieved with various lithographic techniques, the realization of patterned 3D graphene microstructures still remains a significant challenge. Here, a rapid and highly scalable roller-assisted microcontact printing (RAμCP) strategy for the fabrication of 3D graphene oxide micropatterns is reported. The facile RAμCP allows for the robust negative duplication of 3D topologies of the microstructured stamp using chemically modified graphene as the inks. The patterned 3D graphene microstructures exhibit interesting properties of graphene itself and allow for further functionalization of polymers to enable the potential integration of the 3D patterned microstructures into next-generation 2D Janus hybrid thin film for chemical sensors and other electronic devices.

1. Introduction

Graphene, a 2D honeycomb lattice of sp^2-bonded carbon atoms, has received considerable attention for its promising potential applications in sensors,[1] actuators,[2] field-effect transistors,[3] photovoltaic devices,[4] and graphene-based composite materials,[5] because of its unique physical, chemical, and electronic properties. However, to take full advantage of the unique properties of graphene for next-generation devices, a precise fabrication of patterned graphene microstructures is needed. While impressive progress in the development of 2D patterning of graphene with various techniques such as photolithography,[3] interlayer lithography,[6] soft lithography,[7a–d] focused beam technique,[8] and direct writing strategy [9a,b] has been achieved, graphene patterning in 3D is a major challenge. 3D graphene microstructures demonstrate high specific surface and hierarchically vertical geometries, in comparison to the 2D film, the anisotropic 3D microarchitectures have better performance in electrode materials and other electronic devices.[10a,b] A precise, robust, and scalable 3D micropatterning of graphene would open the facile integration of graphene to realize highly sensitive sensors[11] and electrode arrays.[12] Until now, only few reports on the fabrication of 3D patterning of graphene microstructures can be found. For instance, Seol and co-workers[13] reported on the 3D printing of reduced graphene oxide (rGO) nanowire that could be realized by local growth of graphene oxide (GO) using the meniscus formed at the tip of a micropipette with following reduction of GO. Nam and co-workers[10a] integrated graphene thin films into 3D microstructured surfaces via the swelling, shrinking, and adaption of a poly(dimethylsiloxane) (PDMS) stamp to enable the transfer of microstructured graphene. Despite the recent progress, the lack of robustness and scalability of the approaches strongly limits their application for the integration of graphene into novel high-performance devices.

Microcontact printing (μCP),[14] as a simple, versatile, and inexpensive patterning approach, has been used widely to generate various 2D graphene thin film micropatterns.[7c,15a,b] The facile and robust soft lithography techniques were also extended to replica molding,[16] microtransfer molding,[17] micromolding in capillary,[18] and solvent-assisted micromolding[19] for readily realizing 3D micropatterns. However, these fabrication strategies rely on crosslinkable polymers or ceramic precursors and are as such not suitable for the integration of graphene. Based on our long-term endeavor of surface patterning by robust μCP methods,[7c,15a,20a–e] herein we report our recent development to fabricate 3D micropatterns with integrated graphene by the new surface patterning technique of "roller-assisted microcontact printing" (RAμCP) using a GO dispersion as the ink.

P. Xiao, Dr. S. Du, Dr. N. Qiu, Dr. J. Zhang, Dr. Y. Huang, C. Wan, Prof. Q. Huang, Prof. Z. Liu, Prof. T. Chen
Ningbo Institute of Material Technology and Engineering
Key Laboratory of Graphene Technologies and Applications of Zhejiang Province
Chinese Academy of Science
Zhongguan West Road 1219, 315201 Ningbo, China
E-mail: tao.chen@nimte.ac.cn
P. Xiao, Prof. T. Chen
University of Chinese Academy of Science
Beijing 100049, China
Dr. T. Zhang, Prof. R. Jordan
Chair of Macromolecular Chemistry
School of Science
Technische Universität Dresden
Mommsenstr. 4, 01069 Dresden, Germany
E-mail: rainer.jordan@tu-dresden.de

DOI: 10.1002/admi.201600867

RAμCP is a significant advancement of microcontact printing technique and a breakthrough of surface patterning new strategy in fabricating 3D patterned graphene microstructures. The RAμCP performed with apt rolling speed and force allows for the negative duplication and transfer of the 3D topology of stamp into 3D graphene profiles in a single step. Taking advantage of the μCP process, the derived RAμCP can produce 3D micropatterend graphene in a robust and facile fashion, which is highly important for scalable and low cost developments for next-generation graphene-based devices.

2. Results and Discussion

2.1. Roller-Assisted Microcontact Printing

The procedure to fabricate 3D graphene micropatterns by RAµCP is outlined in **Figure 1**a–d. A flexible PDMS stamp with a 3D topography (for example a grid structure) is inked with a dispersion of GO flakes (lateral size ≈5 µm, ≈1.1 nm thickness; Figure 1a, Figure S1a,b, Supporting Information) in ethanol. The GO ink can spread smoothly along the micropatterned PDMS surface with good wettability, forming a homogeneous liquid membrane. After ethanol evaporation, GO flakes spontaneously self-assemble into a thin continuous film that renders its 3D surface topography (Figure 1b). We have reported previously that micropatterned GO with an average thickness of less than 10 nm could be easily transferred in a normal μCP from the GO inked PDMS stamp onto the silicon wafer[7c] (Figure S2a, Supporting Information) because of the strong hydrogen bonding interactions between the hydrophilic GO and the hydroxylated silicon substrate, and interactions between the layered GO flakes within the film (polar, π–π interactions and hydrogen bonding; Figure S1c, Supporting Information).[21] The stamp covered with the continuous GO film is then placed on a substrate (SiO_2) as in a standard µCP process but additionally a roller is applied (Figure 1c) to enable complete transfer of the 3D patterned GO film onto the substrate before the stamp is removed (Figure 1d). We found that for a successful graphene film transfer by the RAµCP, the PDMS stamp must be relatively thin (less than 2 mm) to provide a sufficient stamp flexibility and to induce a viscoelastic deformation of the PDMS stamp by the roller[22] to reduce the PDMS–GO interaction and to facilitate the stamp removal without rupturing the delicate 3D profile of the GO film.

With this simple procedure, RAµCP readily allows the transfer of continuous graphene films with maintained 3D

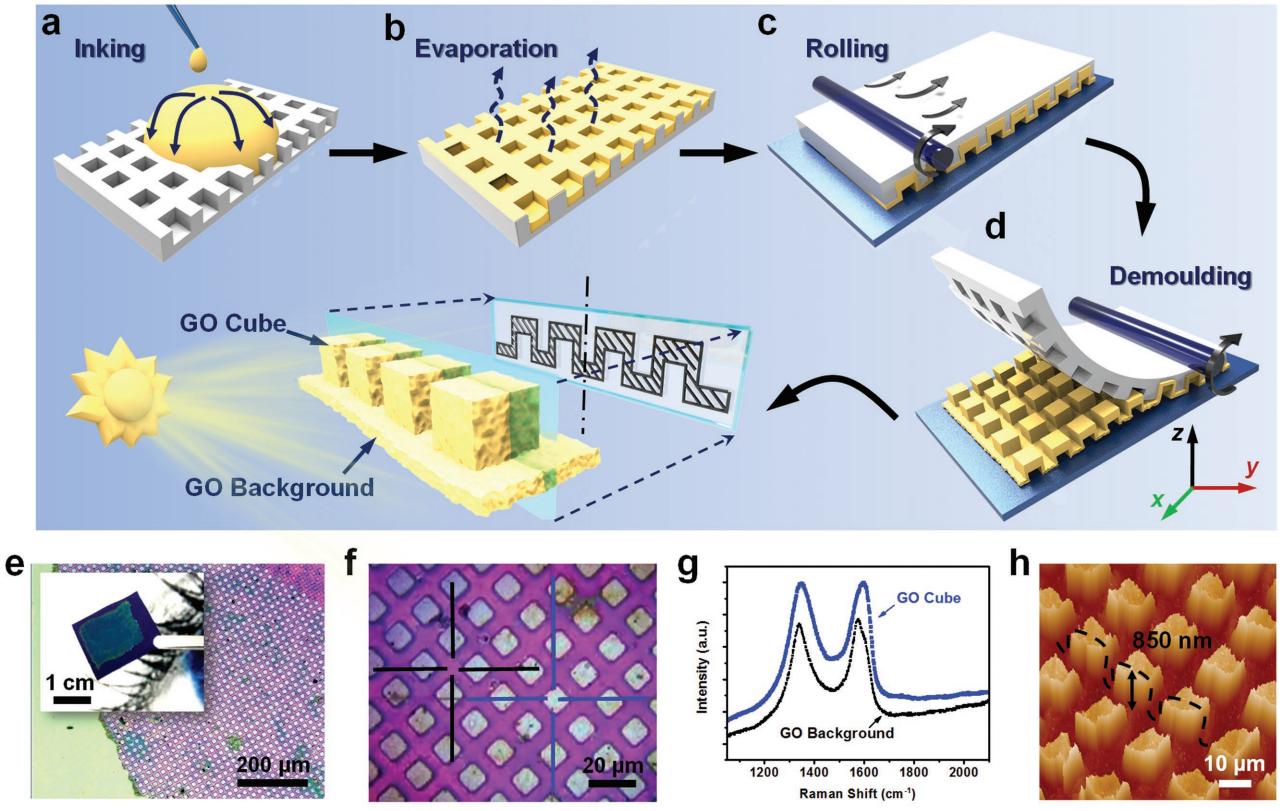

Figure 1. Fabrication of 3D patterned graphene microstructures by roller-assisted microcontact printing (RAμCP). a–d) Schematic illustration of RAμCP process. Stamp inking with a a) GO dispersion, b) solvent evaporation, c) microcontact printing assisted by a roller (≈5 mm in diameter, ≈10 cm in length, and d) the final demoulding transfer of the GO film from stamp onto silicon wafer with maintained 3D profile with velocity ≈1.1 mms^{-1} and pressure ≈3.7 kg. e) Optical image of GO film with cubic architectures. Inset: photograph of the transferred GO film with 3D profile to show its macroscopic lateral size. f) The enlarged optical image of (e). g) Raman spectra of characteristic peaks for the 3D GO cubic structures and GO background corresponding to (f). h) 3D AFM visualization of the cubic structures with an average height around 850 nm. Typically, the aforementioned cubic microstructure is fabricated employing a velocity ≈1.1 mms^{-1} and pressure ≈3.7 kg during RAμCP with GO concentration of ≈3 mg mL^{-1}.

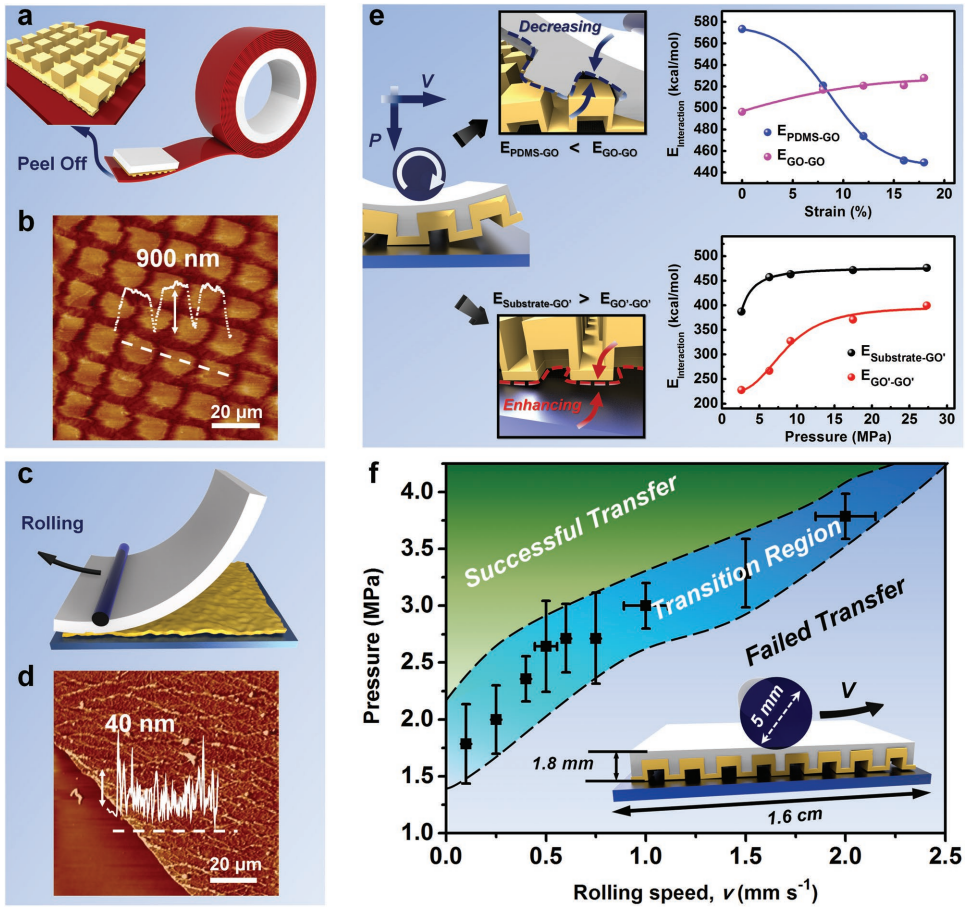

Figure 2. Transfer mechanism of RAμCP. a) Schematic illustration of transferring GO film microprofiles from a PDMS stamp onto an adhesive tape by the Geim-method. b) AFM scan of the transferred 3D GO microtopography with a height of about 900 nm. c) Schematic illustration of the transfer of a GO film from a flat PDMS stamp by RAμCP. d) AFM scan of the transferred GO film with a thickness of ≈40 nm with its typical roughness (inset: section analysis along dashed line). e) The mechanism analysis of the replica demoulding process and simulation curves obtained with Materials Studio software. f) The successful transfer of 3D GO microstructured film with respect to the dependence of the rolling speed and applied pressure (GO concentration is about 3.0 mg mL^{-1}). The error bars are the standard deviation for the rolling speed and applied pressure.

microtopography on cm^2 areas as illustrated by the photograph in the inset of Figure 1e and detailed optical microscopy images (Figure 1e,f). Locally recorded Raman spectroscopy on the GO cube (blue) and GO background (black) revealed the typical characteristic peaks of GO. Investigation of the GO film topography by atomic force microscopy (AFM) showed the 3D microtopography of the graphene with protruding hollow cubes of ≈850 nm height (Figure 1h) and the characteristic wrinkled structure of interconnected GO flakes forming the continuous film (Figure S1d, Supporting Information).

2.2. Transferring Mechanism of RAμCP

For a successful, defect-free transfer of the 3D graphene microtopography from the elastic PDMS stamp onto the substrate, one can enhance the adhesion interaction between the GO film and the receiving target or, alternatively, decrease the interaction between the stamp and the GO film. Inspired by the first example of peeling and transferring of graphene from graphite using an adhesive tape reported by Geim and co-workers,[23] we used a commercial tape to enhance the adhesion energy between the GO and the target substrate to quickly peel the GO film from the stamp in a kinetic control of adhesion (**Figure 2**a).[24] The AFM scan in Figure 2b indicates the successful transfer of a continuous 3D GO film with cubic topography and pattern height around 900 nm, which demonstrates the feasibility of this method. However, further use and application of the transferred pattern on a tape is rather limited. In a recent report by Xie and co-workers,[22] vanadium disulfide (VS_2) nanosheets were readily transferred from a cellulose membrane to arbitrary substrates with the aid of a roller. This transfer process can also be understood as a rolling-induced increase of the adhesion energy between VS_2 and the target, which inspired us to apply this roller-assisted process for the GO film transfer with thicker GO films (≈40 nm) from planar, unpatterned PDMS stamps onto silicon substrates (Figure 2c,d). In contrast to a flat stamp, some area of the structured stamp cannot have a direct contact with the receiving target, resulting in selective patterns and/or incomplete 3D transfer under this operation condition employed on a flat stamp (Figure S2b,c, Supporting Information). Considering the viscoelastic behavior

of PDMS,[16] we induce considerable deformation on the GO inked elastomer which results in incomplete film transfer with a considerable number of cracks (Figure S3, Supporting Information). The deformation of the stamp that effectively decreases the interfacial interaction between PDMS and continuous GO film plays a significant role in the transfer procedure.

Toward exploring the details of transferring process, relationships of different interface energy were first simulated by molecular simulation using COMPASS force field as implemented in Materials Studio software (Figure S4, Supporting Information).[25] Figure 2e shows the schematic models of the rolling process with the three competing interfacial energies defined as $E_{PDMS–GO}$ dominated by the deformation of the stamp, $E_{GO–GO}$ and $E_{Substrate–GO}$ dominated by the applied pressure during the transfer process. In the simulation model, the transfer process can be divided into two parts, which contain the rolling-induced deformation ($E_{PDMS–GO}$ and $E_{GO–GO}$) and pressure-induced enhancement of the adhesion energy ($E_{Substrate–GO'}$ and $E_{GO'–GO'}$). Upon the rolling-induced strained deformation from 0% to 18%, $E_{PDMS–GO}$ decreases from ≈570 to ≈450 kcal mol^{-1}, while $E_{GO–GO}$ increases from ≈500 to ≈530 kcal mol^{-1}. This results in the separation of GO thin film with PDMS stamp. On the other hand, as the increase of rolling pressure from ≈2.6 to ≈27.0 MPa, the adhesion energy of both $E_{Substrate–GO'}$ and $E_{GO'–GO'}$ experiences a prominent increase, showing final values from ≈390 to ≈480 and ≈230 to ≈400 kcal mol^{-1}, respectively. This causes the enhanced adhesion of the GO thin film with target substrate. Eventually, GO nanosheets are highly inclined to be an integrity, which is robust enough to break the PDMS–GO interface and interacts strongly with a receiving target and thus allows the successful transfer of a continuous 3D patterned GO microarchitecture onto the target substrate.

Based on the simulation results, we can now control the RAμCP process by optimization of the transfer parameters such as the applied pressure and rolling speed of roller to realize the 3D graphene micropatterns transfer with a high achievement ratio. With hundreds of trial-and-error cycles we found that slow rolling speed and apt pressure improved the adhesion of the GO film to the silicon substrate and at the same time allowed a defect-free removal of the stamp (Figure S5 and Figure S6, Supporting Information). Phase diagram in detail as shown in Figure 2f shows the dependence of pressure on rolling velocity. As the rolling speed increases from 0.1 to 2 mms^{-1}, the pressure should increase correspondingly (from ≈1.8 to ≈3.8 MPa) to induce sufficient stamp deformation as well as adhesion force for successful transfer of 3D GO micropatterns. The key concept for the successful transfer criteria is that under a certain rolling velocity, the applied pressure value should be larger than that of the transition region. Otherwise, below the critical pressure value, the 3D transfer may fail, resulting in selective patterns or partial 3D microstructures transfer. Furthermore, based on the phase graph, we have further tested the graph through lots of transferring experiments, indicating that the regions are well-defined.

2.3. Morphological Control of 3D Patterned Graphene Oxide Microstructures

The morphology of the transferred 3D graphene microprofiles can be further tuned by the variation of the GO concentration in the dispersion used as the ink. With a concentration of ≈3 mg mL^{-1} and a grid-structured PDMS stamp, the RAμCP results in a 3D GO layer forming hollow microcups (**Figure 3**a). A steady decrease of the GO concentration of the ink results in thinner GO layers of decreasing stability, which causes a transition of the final microarchitectures from turned cups to open double-walled boxes (Figure 3a–d). Importantly, the critical thickness of the box or collapsed one is about 610 nm with the critical concentration of ≈2 mg mL^{-1}. The box structures are formed by the collapse of the suspended upper GO film (Figure 3e). Interestingly, the height of the box walls is linearly dependent on the GO ink concentration (Figure 3f). As apparent from the cross-section analysis of the AFM scans (Figure S7, Supporting Information), all 3D GO arrays have a continuous GO background, indicating an integral material with ordered embossment. Further investigations of the 3D GO microarray by scanning electron microscopy (SEM) (Figure 3g,h and Figure S8, Supporting Information) revealed that the large and uniform array is flexible and can be detached from the supporting substrate without losing its integrity.

To demonstrate the universality of RAμCP, stamps with various structures and structural dimensions were used for the fabrication of patterned 3D GO microarrays on a large scale (Figure S9, Supporting Information). Readily, arrays of dots, grids, rings, and lines could be easily fabricated and all with a continuous GO film forming the profile (**Figure 4**a–d, Figure S10, Supporting Information). Notably, highly concentrated GO ink and line shaped stamps resulted in 3D arrays with heights on the submicrometer scale (Figure 4e,f). With dilution of the GO ink, line arrays of adjustable spacing and heights can be produced with the same stamp (Figure 4g–i). It is noted that the minimum features of 3D graphene patterns depend strongly on the lateral size of GO nanosheets. In our system, the minimum size could be achieved successfully around 2 μm (Figure 4h,i and Figure S11, Supporting Information). However, it is supposed that 3D GO feature size could be minimized to submicron level with appropriate GO sheets sizes. Furthermore, we found that even macroscopic objects can be reliably transformed into 3D GO reliefs. This is demonstrated by the use of various coins as a master to cast the PDMS stamp, which in turn is then used to produce 3D GO patterns by RAμCP (Figure S12, Supporting Information).

2.4. Fabrication of 2D Janus Hybrids and Their Electrical Performance for Flexible Electronics

Since GO as well as graphene can be readily functionalized by various chemical reactions,[26a,b] the chemical and physical properties of the 3D GO micro- and macroreliefs, fabricated by RAμCP, can be broadly tuned. Especially the functionalization by a defined polymer layer such as a polymer brush is of high technological interest.[27] For the grafting of polymer brushes onto carbonaceous material, the self-initiated photografting and photopolymerization (SIPGP) is the most direct and efficient method as it is applicable to a wide variety of vinyl monomers and does not require an initiator precoating.[28a–d,7c,29] As an example, a 3D GO array featuring open boxes with a wall height around 180 nm (**Figure 5**a) was grafted with a

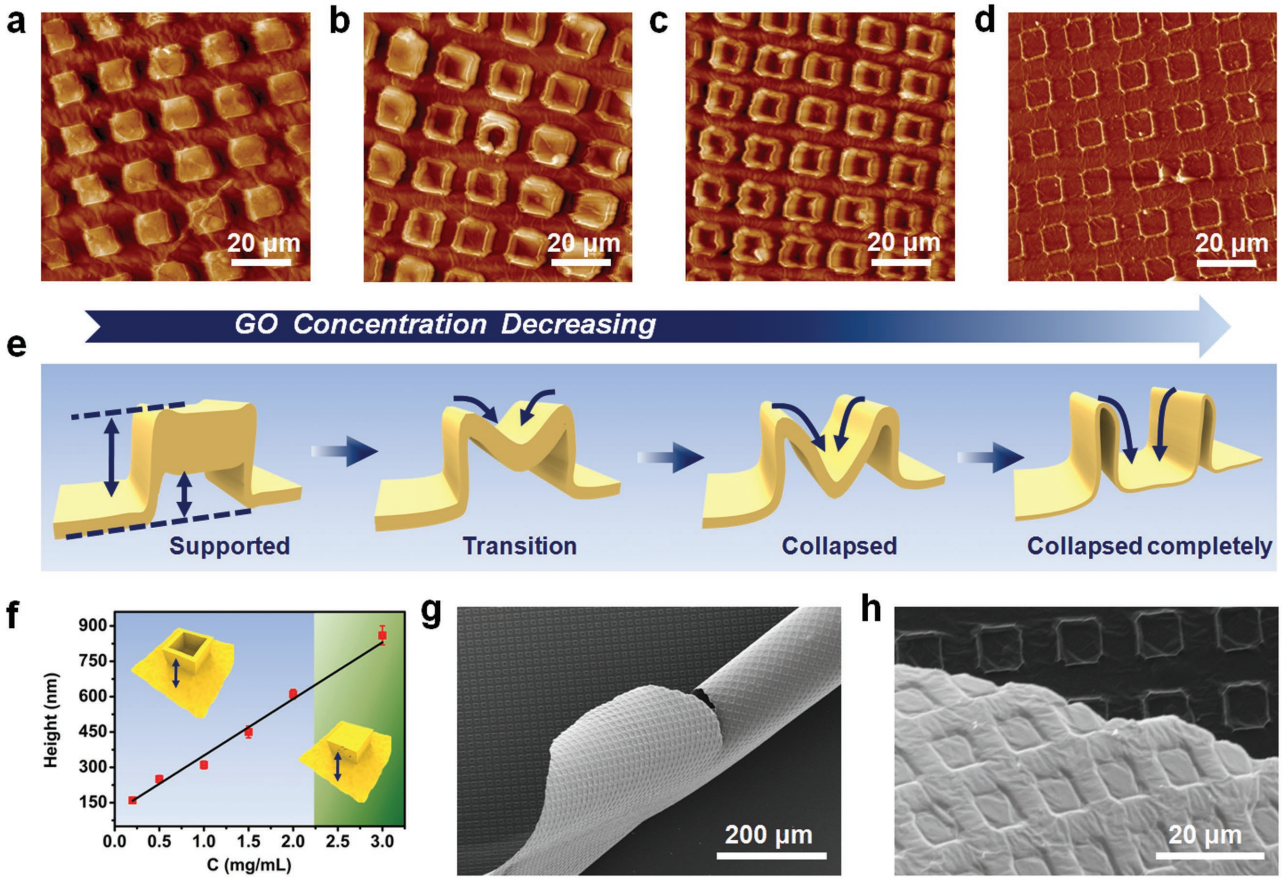

Figure 3. 3D patterned graphene microprofiles with controlled shapes (PDMS features: grid-shaped size ≈4.5 µm, ≈10 µm spacing, and ≈1 µm in depth). a) AFM scan of an array of hollow upside-down boxes transferred by RAµCP using a GO ink concentration of C = 3 mg mL^{-1}, b) with lower GO concentration (C = 2 mg mL^{-1}) the same process results in partly collapsed structures and further decrease of the concentration results in open double-walled boxes at c) C = 1.5 and d) C = 1 mg mL^{-1}. e) The section illustration of morphology transition. f) Wall height of the boxes as a function of the GO concentration of the ink solution. g) Partially detached microbox array illustrating the flexibility and robustness of the array. h) Detailed SEM micrograph showing the bottom and top side of the box array fabricated by RAµCP with a rolling pressure of ≈3.7 kg and velocity of ≈1.1 mms^{-1}.

poly(N,N-dimethylaminoethylmethacrylate) (PDMAEMA) brush by SIPGP. The added brush layer increased the wall height from original 180 to 400 nm and the walls became noticeably broader (Figure 5b,c). The polymer brush coating also significantly changed the wetting properties of the 3D GO array with a water contact angle of 74 ± 2° (native) to 28 ± 1° for the GO-PDMAEMA brush composite (Figure 5d). It is noteworthy that with this approach, only one side of the GO film is functionalized by the brush and therefore, Janus-type 3D microstructured reliefs are produced.[30a,b] The additional brush layer further stabilizes the relief and allowed a complete detachment from the support (Figure 5e, Figure S13a,b, Supporting Information). The free-standing 3D GO reliefs are highly flexible, yet robust enough to fold without rupture (Figure S13c,d, Supporting Information).

Since the SIPGP is a photografting reaction using UV light, the GO layer is grafted with the polymer as well as converted to rGO which is a good conductor.[31] This is evidenced by conductivity measurements of the 3D GO relief and the GO-PDMAEMA hybrid. While the first is an isolator, the latter displays a linear *I–V* curve on Au electrodes with thickness of about 50 nm spaced by 550 µm indicating an ohmic contact (Figure 5f,g). Due to the specific features of the Au electrodes on glass target, the hybrid can spread smoothly and tightly along the target surface. The rGO-PDMAEMA had a maximum current of ≈0.53 mA at the bias of –1.0 and 1.0 V which calculates to a conductivity of 1325 S m^{-1}. Transient response by sustained voltage pulses of a width of 1 s and amplitude of 0.5 V is shown in Figure 5h, which exhibits a good reproducibility. The promising electrical properties, together with the 3D shaping of the rGO film and the functionalization with a broad variety of polymer brushes are an ideal combination for the development of functional materials for various (bio)sensor applications and actuators.

3. Conclusion

In summary, we reported a new, rapid, facile, and highly scalable direct surface patterning strategy of roller-assisted microcontact printing (RA*µ*CP) for the preparation of patterned graphene films in 3D. This new technique, assisted by a roller during *µ*CP, can entirely allow the robust duplication and transferring of GO film with 3D negative topologies of

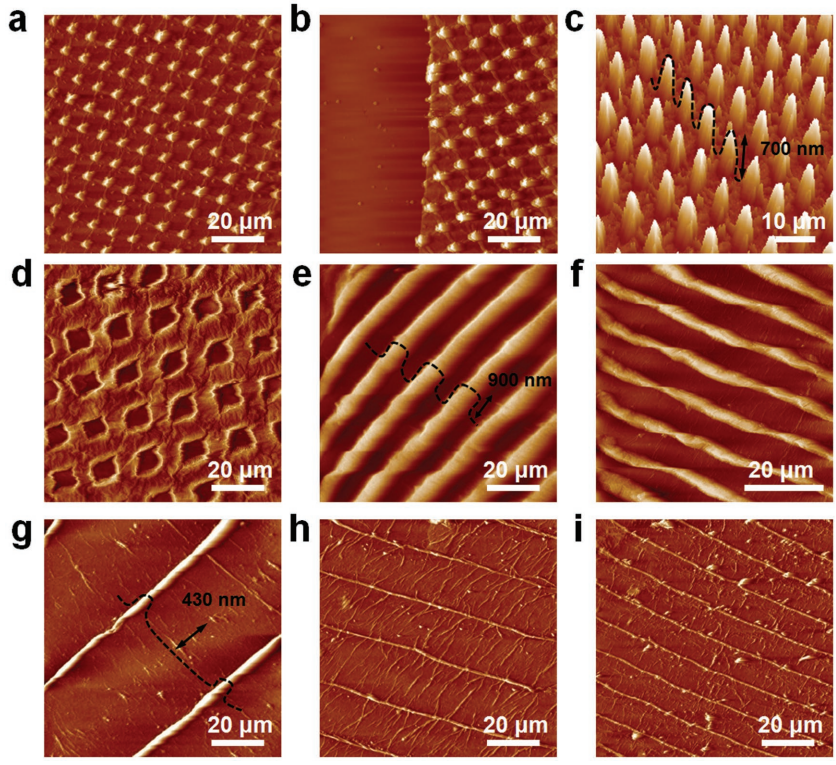

Figure 4. AFM images of 3D patterned graphene microstructures with various shapes. a,b) Dotted arrays, PDMS features: grid-shaped size ≈2.5 μm, ≈5 μm spacing, and ≈1 μm in depth. c) 3D view of dotted arrays. d) Grid arrays, PDMS features: cubic-shaped size ≈10 μm, ≈4.5 μm spacing, and ≈1 μm in depth. Various line arrays fabricated by line-shaped stamp with different width. e) PDMS features: Line-shaped size ≈10 μm, ≈10 μm spacing, and ≈1 μm in depth, f) line-shaped size ≈5 μm, ≈5 μm spacing, and ≈1 μm in depth. Low concentration of less than 1.5 mg mL^{-1}, g) 20, h) 10, and i) 5 μm.

the stamp microstructures during the μCP. RAμCP is a significant advancement of microcontact printing technique and a breakthrough of surface patterning new strategy in fabricating 3D patterned graphene microstructures. Taking advantage of the μCP process, the derived RAμCP can produce 3D micropatterend graphene in a robust fashion with low cost. Our patterning technique is readily suited for use in automated printing machines and has the potential to fabricate other various 2D functional materials in 3D on a wide range of substrates with controlled size, shape, and morphology. The patterned 3D graphene microstructures allow for further functionalization of polymers to enable the integration of the 3D patterned microstructures into next-generation 2D Janus hybrid thin film for chemical sensors and other electronic devices.

4. Experimental Section

Materials: General chemicals in chemical reagent grade were used as received from Sinopharm Chemical Reagent. Ethanol and deionized water were used as rinsing solvents. *N,N*-dimethylaminoethylmethacrylate was obtained from Alfa Aesar China (Tianjin) Co., Ltd, which was purified by neutral Al_2O_3 column and dried with a 0.4 nm molecular sieve at room temperature for 3 d. PDMS stamps with grid, cubic, and line-shaped structures were fabricated from Sylgard 184 (the ratio between component A and B was 1:10) at 70 °C for 2 h on a silicon master. PDMS stamp was used without any pre-treatment. Silicon wafers were cleaned in a mixture of H_2O_2/H_2SO_4 (1:3,v/v) at 80 °C ("piranha solution") for 2 h and washed thoroughly with Milli-Q-grade water (Caution: Piranha solution reacts violently with organic matter!).

Preparation of Homogeneous Dispersion GO Aqueous Solution: GO sheets were synthesized by a modified Hummers' method[32] and exfoliation of graphite oxide was achieved by a strong ultrasonication method. The obtained brown dispersion was then washed and centrifuged to remove any unexfoliated graphite oxide.

Preparation of 3D Patterned Graphene Microarchitectures by RAμCP: The PDMS stamp was inked by exposing the stamp features to an ethanol solution of GO until the solvent dried. A roller was employed to roll across the structured PDMS with slow velocity and apt pressure. The operation parameters were systematically adjusted by conducting amounts of experiments. The pressure was measured by a platform balance, which can reach the accuracy of 1 g. The velocity was measured by a stopwatch and ruler.

SIPGP: The patterned 3D GO microstructures substrate was submerged in ≈2 mL of distilled and degassed monomer and irradiated with a UV lamp with a spectral distribution between 300 and 400 nm distribution (intensity maximum at λ = 365 nm with a total power of ≈240 mW cm^{-2}) for required time of about 50 min. Following SIPGP (M. Steenackers, A. Kuller, S. Stoycheva, M. Grunze, R. Jordan, *Langmuir*2009, *25*, 2225.), the functionalized films were exhaustively rinsed with ethanol following ultrasonication for several minutes in order to remove any physisorbed PDMAEMA.

Fabrication of Freestanding Patterned Films: The patterned polymer brushes grafted 3D patterned GO microarchitectures were cleaved from the silicon surface by immersing the silicon wafer in NaOH solution (1 M) overnight.

Characterization: AFM images were taken by a multimode AFM (Being Nano-Instruments, Ltd) operating in the contact and/or tapping mode using silicon cantilevers (spring constant: 0.15 Nm^{-1}, resonant frequency: 12 KHz for cantilever of contact mode, spring constant: 3–40 Nm^{-1}, resonant frequency: 75–300 KHz for cantilever of tapping mode). Static water contact angles were measured at room temperature using the sessile drop method and image analysis of the drop profile. The instrument (OCA-20, Dataphysics) used a charge-coupled device camera and an image analysis processor. The water (Milli-Q) droplet volume was 3 μL, and the contact angle was measured after the drop was stable on the sample. For each sample, the reported value was the average of the results obtained on three droplets. Optical images were acquired by polarized optical microscopy (Olympus, BX 51TF Instec H601). The Raman scattering measurements were performed at room temperature on a Raman system (inVia-reflex, Renishaw) with confocal microscopy. The solid-state diode laser (532 nm) was used as an excitation source with a frequency range of 3200–1000 cm^{-1}. Electrical measurements of devices were performed with a semiconductor parameter analyzer (Keithley 4200). Field emission scanning electron microscope images were obtained with a FE scanning electron microanalyzer (Hitachi-S4800, 4 kV).

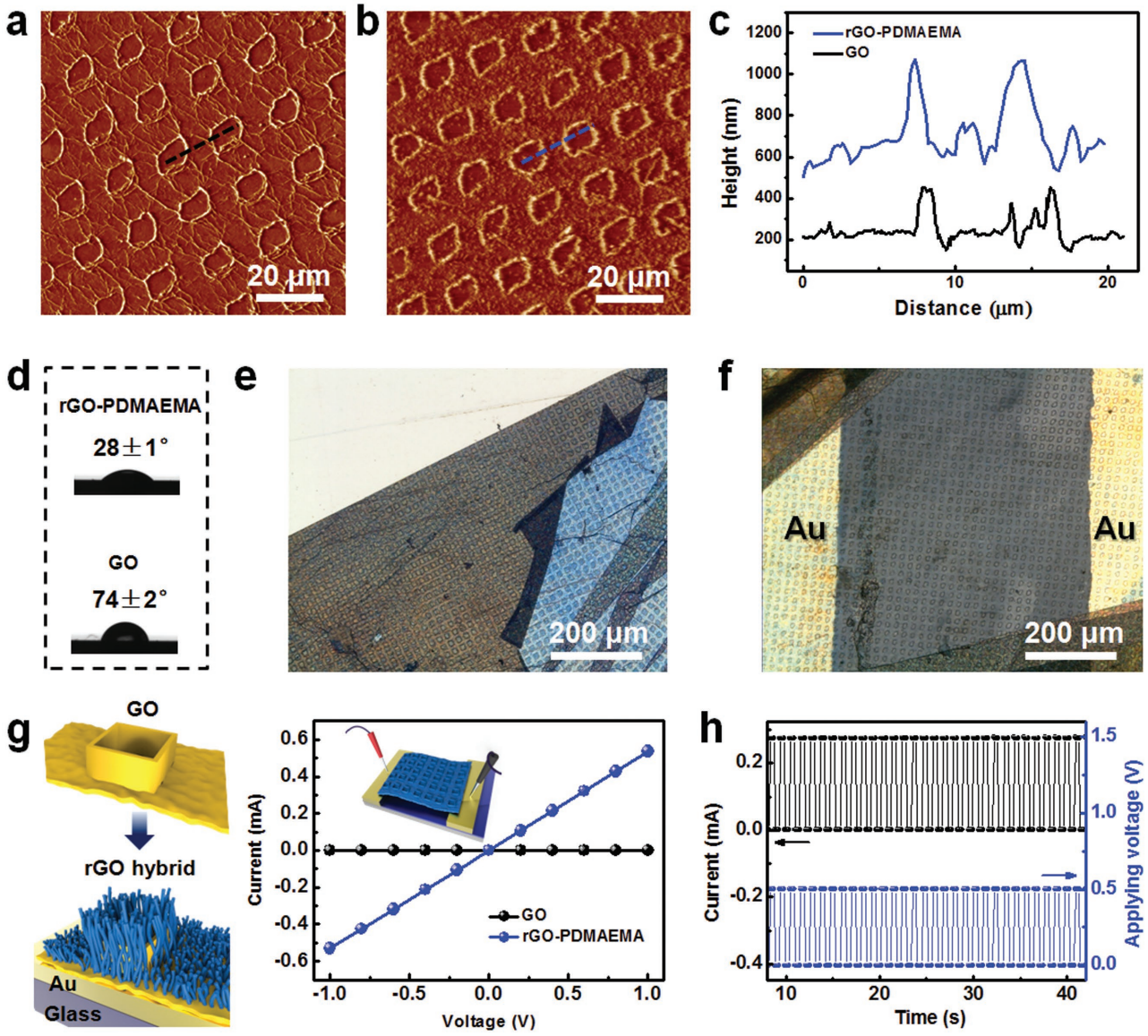

Figure 5. Polymer brushes functionalized 3D graphene architectures and properties characterization. a) AFM scan of GO ring structures. b) PDMAEMA-functionalized rGO ring structures. c) AFM height profiles of the ring height before and SIPGP. d) Water contact angle values of the 3D GO ring structures before and after SIPGP. e) Optical image of free-standing PDMAEMA-functionalized rGO film with 3D ring architectures transferred onto glass substrate. f) Optical image of free-standing PDMAEMA-functionalized RGO ring structures transferred onto the patterned Au electrodes surface for further electrical measurements. g) Schematic of GO and polymer grafted GO, current–voltage curves of the free-standing 3D ring structures and polymer functionalized ones in air. h) *I–t* and *ν–t* curves of transient response, at 1 s for each cycle.

Supporting Information

Supporting Information is available from the Wiley Online Library or from the author.

Received: September 8, 2016
Revised: October 10, 2016
Published online:

Acknowledgements

The authors thank the Natural Science Foundation of China (51573203, 51303195), the Bureau of Frontier Science and Education of Chinese Academy of Sciences (QYZDB-SSW-SLH036), Excellent Youth Foundation of Zhejiang Province of China (LR14B040001), Ningbo Science and Technology Bureau (2014B82010, 2015C110031), and Youth Innovation Promotion Association of Chinese Academy of Science (2016268).

[1] F. Schedin, A. K. Geim, S. V. Morozov, E. W. Hill, P. Blake, M. I. Katsnelson, K. S. Novoselov, *Nat. Mater.* **2007**, *6*, 652.
[2] X. J. Xie, L. T. Qu, C. Zhou, Y. Li, J. Zhu, H. Bai, G. Q. Shi, L. M. Dai, *ACS Nano* **2010**, *4*, 6050.

[3] S. Pang, H. N. Tsao, X. Feng, K. Muellen, *Adv. Mater.* **2009**, *21*, 3488.
[4] Y. Wang, X. Chen, Y. Zhong, F. Zhu, K. P. Loh, *Appl. Phys. Lett.* **2009**, *95*, 063302.
[5] S. Stankovich, D. A. Dikin, G. H. B. Dommett, K. M. Kohlhaas, E. J. Zimney, E. A. Stach, R. D. Piner, S. T. Nguyen, R. S. Ruoff, *Nature* **2006**, *442*, 282.
[6] P. H. Wöbkenberg, G. Eda, D.-S. Leem, J. C. de Mello, D. D. C. Bradley, M. Chhowalla, T. D. Anthopoulos, *Adv. Mater.* **2011**, *23*, 1558.
[7] a) M. J. Allen, V. C. Tung, L. Gomez, Z. Xu, L.-M. Chen, K. S. Nelson, C. Zhou, R. B. Kaner, Y. Yang, *Adv. Mater.* **2009**, *21*, 2098; b) Q. He, H. G. Sudibya, Z. Yin, S. Wu, H. Li, F. Boey, W. Huang, P. Chen, H. Zhang, *ACS Nano* **2010**, *4*, 3201; c) P. Xiao, J. Gu, J. Chen, J. Zhang, R. Xing, Y. Han, J. Fu, W. Wang, T. Chen, *Chem. Commun.* **2014**, *50*, 7103; d) P. Xiao, J. Gu, J. Chen, D. Han, J. Zhang, H. Cao, R. Xing, Y. Han, W. Wang, T. Chen, *Chem. Commun.* **2013**, *49*, 11167.
[8] Y. Zhou, Q. Bao, B. Varghese, L. A. L. Tang, C. K. Tan, C.-H. Sow, K. P. Loh, *Adv. Mater.* **2010**, *22*, 67.
[9] a) K. Salaita, Y. Wang, C. A. Mirkin, *Nat. Nano* **2007**, *2*, 145; b) K.-Y. Shin, J.-Y. Hong, J. Jang, *Adv. Mater.* **2011**, *23*, 2113.
[10] a) J. Choi, H. J. Kim, M. C. Wang, J. Leem, W. P. King, S. Nam, *Nano Lett.* **2015**, *15*, 4525; b) J. H. Park, D. H. Cho, Y. Moon, H. C. Shin, S. J. Ahn, S. K. Kwak, H. J. Shin, C. Lee, J. R. Ahn, *ACS Nano* **2014**, *8*, 11657.
[11] B. Tian, J. Liu, T. Dvir, L. Jin, J. H. Tsui, Q. Qing, Z. Suo, R. Langer, D. S. Kohane, C. M. Lieber, *Nat. Mater.* **2012**, *11*, 986.
[12] D.-W. Park, A. A. Schendel, S. Mikael, S. K. Brodnick, T. J. Richner, J. P. Ness, M. R. Hayat, F. Atry, S. T. Frye, R. Pashaie, S. Thongpang, Z. Ma, J. C. Williams, *Nat. Commun.* **2014**, *5*, 5258.
[13] J. H. Kim, W. S. Chang, D. Kim, J. R. Yang, J. T. Han, G.-W. Lee, J. T. Kim, S. K. Seol, *Adv. Mater.* **2015**, *27*, 157.
[14] Y. N. Xia, G. M. Whitesides, *J. Am. Chem. Soc.* **1995**, *117*, 3274.
[15] a) P. Xiao, C. Wan, J. Gu, Z. Liu, Y. Men, Y. Huang, J. Zhang, L. Zhu, T. Chen, *Adv. Funct. Mater.* **2015**, *25*, 2428; b) A. Carlson, A. M. Bowen, Y. G. Huang, R. G. Nuzzo, J. A. Rogers, *Adv. Mater.* **2012**, *24*, 5284.
[16] Y. N. Xia, E. Kim, X. M. Zhao, J. A. Rogers, M. Prentiss, G. M. Whitesides, *Science* **1996**, *273*, 347.
[17] X. M. Zhao, Y. N. Xia, G. M. Whitesides, *Adv. Mater.* **1996**, *8*, 837.
[18] Y. N. Xia, E. Kim, G. M. Whitesides, *Chem. Mater.* **1996**, *8*, 1558.
[19] E. Kim, Y. N. Xia, X. M. Zhao, G. M. Whitesides, *Adv. Mater.* **1997**, *9*, 651.
[20] a) P. Xiao, J. Gu, J. Chen, D. Han, J. Zhang, H. Cao, R. Xing, Y. Han, W. Wang, T. Chen, *Chem. Commun.* **2013**, *49*, 11167; b) T. Chen, R. Jordan, S. Zauscher, *Small* **2011**, *7*, 2148; c) T. Chen, R. Jordan, S. Zauscher, *Polymer* **2011**, *52*, 2461; d) T. Chen, D. P. Chang, S. Zauscher, *Small* **2010**, *6*, 1504; e) T. Chen, J. Zhong, D. P. Chang, A. Carcia, S. Zauscher, *Adv. Mater.* **2009**, *21*, 1825.
[21] J. Kim, L. J. Cote, F. Kim, W. Yuan, K. R. Shull, J. Huang, *J. Am. Chem. Soc.* **2010**, *132*, 8180.
[22] J. Feng, L. Peng, C. Wu, X. Sun, S. Hu, C. Lin, J. Dai, J. Yang, Y. Xie, *Adv. Mater.* **2012**, *24*, 1969.
[23] K. S. Novoselov, A. K. Geim, S. V. Morozov, D. Jiang, Y. Zhang, S. V. Dubonos, I. V. Grigorieva, A. A. Firsov, *Science* **2004**, *306*, 666.
[24] M. A. Meitl, Z. T. Zhu, V. Kumar, K. J. Lee, X. Feng, Y. Y. Huang, I. Adesida, R. G. Nuzzo, J. A. Rogers, *Nat. Mater.* **2006**, *5*, 33.
[25] H. Sun, P. Ren, J. R. Fried, *Comput. Theor. Polym. Sci.* **1998**, *8*, 229.
[26] a) V. Georgakilas, M. Otyepka, A. B. Bourlinos, V. Chandra, N. Kim, K. C. Kemp, P. Hobza, R. Zboril, K. S. Kim, *Chem. Rev.* **2012**, *112*, 6156; b) D. Chen, H. Feng, J. Li, *Chem. Rev.* **2012**, *112*, 6027.
[27] D. Wang, G. Ye, X. Wang, X. Wang, *Adv. Mater.* **2011**, *23*, 1122.
[28] a) M. Steenackers, A. Kuller, S. Stoycheva, M. Grunze, R. Jordan, *Langmuir* **2009**, *25*, 2225; b) M. Steenackers, A. M. Gigler, N. Zhang, F. Deubel, M. Seifert, L. H. Hess, C. Lim, K. P. Loh, J. A. Garrido, R. Jordan, M. Stutzmann, I. D. Sharp, *J. Am. Chem. Soc.* **2011**, *133*, 10490; c) P. Xiao, J. Gu, J. He, S. Wang, J. Zhang, Y. Huang, S. Kuo, T. Chen, *J. Mater. Chem. C* **2016**, *4*, 9750; d) P. Xiao, J. Gu, C. Wan, S. Wang, J. He, J. Zhang, Y. Huang, S. Kuo, T. Chen, *Chem. Mater.* **2016**, *28*, 7125.
[29] M. Steenackers, R. Jordan, A. Kuller, M. Grunze, *Adv. Mater.* **2009**, *21*, 2921.
[30] a) F. Liang, C. Zhang, Z. Yang, *Adv. Mater.* **2014**, *26*, 6944; b) A. Walther, A. H. E. Müller, *Chem. Rev.* **2013**, *113*, 5194.
[31] L. J. Cote, R. Cruz-Silva, J. Huang, *J. Am. Chem. Soc.* **2009**, *131*, 11027.
[32] W. S. Hummers, R. E. Offeman, *J. Am. Chem. Soc.* **1958**, *80*, 1339.